Journal of Magnetic Resonance 214 (2012) 289–295

Contents lists available at SciVerse ScienceDirect

Journal of Magnetic Resonance

journal homepage: www.elsevier.com/locate/jmr

High-resolution absorptive intermolecular multiple-quantum coherence NMR spectroscopy under inhomogeneous fields

Meijin Lin [a,b], Yanqin Lin [a], Xi Chen [a,*], Shuhui Cai [a], Zhong Chen [a,*]

[a] Department of Electronic Science, Fujian Provincial Key Laboratory of Plasma and Magnetic Resonance, State Key Laboratory of Physical Chemistry of Solid Surfaces, Xiamen University, Xiamen 361005, China
[b] Department of Oceanography, Key Laboratory of Underwater Acoustic Communication and Marine Information Technology, Ministry of Education, Xiamen University, Xiamen 361005, China

ARTICLE INFO

Article history:
Received 5 September 2011
Available online 10 December 2011

Keywords:
High-resolution
Absorption lineshape
Strong coupling artifact
Intermolecular multiple-quantum coherences
Inhomogeneous fields

ABSTRACT

Intermolecular multiple-quantum coherence (iMQC) is capable of improving NMR spectral resolution using a 2D shearing manipulation method. A pulse sequence termed CT-iDH, which combines intermolecular double-quantum filter (iDQF) with a modified constant-time (CT) scheme, is designed to achieve fast acquisition of high-resolution intermolecular zero-quantum coherences (iZQCs) and intermolecular double-quantum coherences (iDQCs) spectra without strong coupling artifacts. Furthermore, double-absorption lineshapes are first realized in 2D intermolecular multi-quantum coherences (iMQCs) spectra under inhomogeneous fields through a combination of iZQC and iDQC signals to double the resolution without loss of sensitivity. Theoretically the spectral linewidth can be further reduced by half compared to original iMQC high-resolution spectra. Several experiments were performed to test the feasibility of the new method and the improvements are evaluated quantitatively. The study suggests potential applications for *in vivo* spectroscopy.

1. Introduction

High-resolution NMR spectroscopy can provide valuable information for structure elucidation. In many cases, however, high-resolution spectra are virtually impossible to obtain because of the inherent heterogeneity of the samples or living organisms under investigation, as well as the poor homogeneity of the magnets. Therefore, there is a great deal of interest and excitement in exploring high-resolution NMR techniques in inhomogeneous fields. Nutation echoes [1,2], shim pulses [3] and modified horse-shoe magnet [4] were utilized to obtain chemical shift information under highly inhomogeneous magnetic fields [5]. A method based on coherence transfer between spins was proposed to obtain high-resolution NMR spectra in inhomogeneous field with unknown spatio-temporal variations [6]. More recently, a new shimming approach was implemented on a pocket-size permanent magnet to obtain high-resolution spectroscopy of conventional samples [7]. Intermolecular multiple-quantum coherences (iMQCs) originating from distant dipolar interactions between spins [8] are capable of improving NMR spectral resolution when magnetic field inhomogeneities vary over distances much larger than the distances between coupled spins [9]. Several magnetic resonance spectroscopic techniques that use iMQCs to refocus inhomogeneous line broadening have been proposed [10–17].

Unfortunately, the usefulness of existing 2D iMQC high-resolution methods is considerably reduced by several drawbacks. Firstly, none of the 2D iMQC spectra has double-absorption mode hitherto. The signals are phase-modulated, therefore absolute-value spectra are usually used for high-resolution projection, which introduces unfavorable line broadening [18,19]. Secondly, strong scalar couplings lead to additional cross-peaks generally known as "strong coupling artifacts" [20], which make the projection of a 2D spectrum more crowded or distort the relative intensities of components in a strongly coupled multiplet, and make the spectral interpretation ambiguous, especially for a closely spaced spectrum. The extra peaks are immune from coherence selection, as they have the same coherence transfer pathway (CTP) as the desired ones. Thrippleton and co-workers proposed two methods to suppress the undesired strong coupling artifacts: one utilizes a double spin echo sequence with constant total echo time and averaged sub-echo times, while another is on the basis of symmetrization procedure [21].

In current work, we propose a pulse sequence to overcome the above two drawbacks of iMQC high-resolution spectroscopy. The proposed sequence, which is termed CT-iDH (see Fig. 1b), combines the iDQF-HOMOGENIZED (abbreviated as iDH) sequence [14,15] with a modified constant-time (CT) scheme [22]. The CT scheme with a fixed evolution period is modified in the proposed

* Corresponding authors. Fax: +86 592 2189426.
E-mail addresses: xichen.nmr@gmail.com (X. Chen), chenz@xmu.edu.cn (Z. Chen).

1090-7807/$ - see front matter © 2011 Elsevier Inc. All rights reserved.
doi:10.1016/j.jmr.2011.12.003

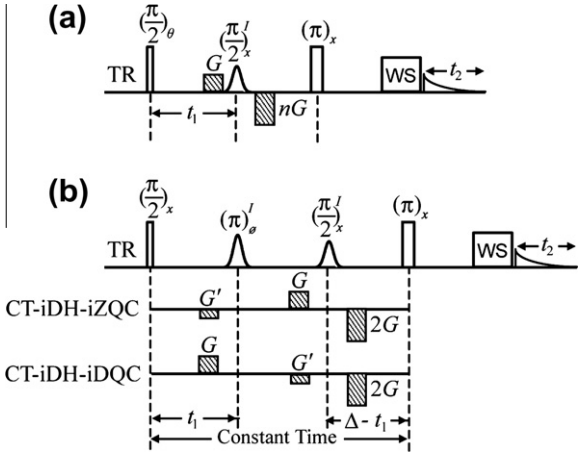

Fig. 1. Pulse sequences: (a) original iZQC ($n = 0$)/iDQC ($n = 2$) sequence [9,10], and (b) CT-iDH sequence.

sequence to eliminate the strong coupling artifacts. The CT-iDH sequence inherits the module of iDQF from the iDH, not only to suppress solvent signal [14], but also to achieve mirror pathways to eliminate the dispersion component. For the first time, the double-absorption lineshape is realized in 2D iMQC spectra under inhomogeneous fields. Furthermore, the manipulation of the t_1 period achieves narrow spectral width in indirect dimension without any loss of information. The sparse sampling in the indirect dimension speeds up the acquisition of 2D spectroscopy, making the new method more applicable in *in vivo* studies.

2. Theories and methods

2.1. Obtaining double-absorption spectra

To obtain absorption spectra, our idea is to record two equally weighted signals with mirror image pathways [23]. In the CT-iDH sequence (Fig. 1b), the CTP $0 \to 0$ (iZQC) $\to +2$ (iDQC) $\to +1 \to -1$ was selected. iZQC and iDQC periods were utilized in the mirror pathways, respectively. They are dubbed as CT-iDH-iZQC and CT-iDH-iDQC (Fig. 1b). These two complementary spectra, which are almost equal in amplitude and symmetric about ω_1 or $t_1 = 0$, are independently collected. Although either spectrum has undesirable phase-twisted lineshape, they can always be combined via data processing to form a complete echo in both dimensions of time domain, thus yielding a 2D amplitude-modulated spectrum in frequency domain. Before Fourier transformation (FT), one of the datasets is mirror imaged with respect to $t_1 = 0$, and then added with its complementary one. (Or, after FT, the ω_1 axis of one of the spectra is reversed, and then the two spectra are added together.) It turns out that the dispersive parts of the phase-twisted lineshape are canceled. Thus, an absorption spectrum can be obtained.

In the following theoretical deduction, we will consider a well-mixed liquid sample, consisting of solvent spin I and solute spin S, both of which are single spin-1/2 systems. It is assumed that I spin is abundant and S spin are either abundant or dilute. The two CTPs of the CT-iDH sequence can be interpreted by using the raising and lowing operator formalism:

$$I_zS_z \overset{\frac{\pi}{2}I_x,\frac{\pi}{2}S_x}{\to} \begin{cases} I^-S^+ \\ I^+S^+ \end{cases} (\tau_1+t_1) \overset{\pi I_x}{\to} \begin{cases} I^+S^+ \\ I^-S^+ \end{cases} (\tau_2) \overset{\frac{\pi}{2}I_x}{\to} I_zS^+(\tau_3-t_1) \overset{\pi I_x,\pi S_x,D_{IS}I_zS_zt_2}{\to} S^-(\tau_4+t_2), \tag{1}$$

where τ_1, τ_2, τ_3 and τ_4 are constants, and $\tau_3 \geqslant t_{1\max}$. In the CT-iDH sequence, evolution period includes an interval $\tau_1 + t_1$ and an interval $\tau_3 - t_1$. We assume ω_m is the frequency offset of spin m ($m = I, S$) in the rotating frame in the absence of magnetic field inhomogeneity, and $\Delta\omega$ is the deviation of the angular frequency caused by magnetic field inhomogeneity, then the frequency offset of spin m is

$$\Omega_m = \omega_m + \Delta\omega, \quad m = I, S. \tag{2}$$

The CT-iDH sequence leads to the chemical shifts of solvent–solute cross-peaks at

$$\begin{aligned} &\text{CT-iDH-iZQC}: (\Omega_1,\Omega_2) = [(-\Omega_I+\Omega_S)-\Omega_S,\Omega_S] = (-\Omega_I,\Omega_S); \\ &\text{CT-iDH-iDQC}: (\Omega_1,\Omega_2) = [(+\Omega_I+\Omega_S)-\Omega_S,\Omega_S] = (+\Omega_I,\Omega_S), \end{aligned} \tag{3}$$

which shows that the resonances of iZQC and iDQC appear in pair symmetric about $\omega_1 = 0$. Note that only the frequency offset of solvent causes the t_1 modulation. Therefore, the 2D spectra can be recorded in very short scan time.

For convenience in the following deduction, we neglect the initial time-increasing (or growth) FID magnitude modulation caused by distant dipolar field (DDF), and assume $\tau_1 = \tau_2 = \tau_4 = 0$, and $\tau_3 = t_{1\max}$. Considering the frequency offsets and the transverse relaxation, the t_1 and t_2 dependences of the CT-iDH-iZQC signal can be deduced as:

$$\begin{aligned} &I_zS_z \overset{\frac{\pi}{2}I_x,\frac{\pi}{2}S_x}{\to} \frac{1}{4}I^-S^+ \overset{t_1}{\to} \frac{1}{4}I^-S^+ \exp[i(\Omega_S-\Omega_I)t_1] \\ &\times \exp\left[-\left(R_2^I+R_2^S\right)t_1\right] \overset{\pi I_x}{\to} \frac{1}{4}I^+S^+ \exp[i(\Omega_S-\Omega_I)t_1] \\ &\times \exp\left[-\left(R_2^I+R_2^S\right)t_1\right] \overset{\frac{\pi}{2}I_x}{\to} \frac{i}{4}I_zS^+ \exp[i(\Omega_S-\Omega_I)t_1] \\ &\times \exp\left[-\left(R_2^I+R_2^S\right)t_1\right] \overset{-t_1}{\to} \frac{i}{4}I_zS^+ \exp(-i\Omega_It_1) \\ &\times \exp\left(-R_2^It_1\right) \overset{\pi I_x,\pi I_x,t_2}{\to} \frac{i}{4}I_zS^- \exp(-i\Omega_It_1) \\ &\times \exp\left(-R_2^It_1\right) \exp(-i\Omega_St_2) \exp\left(-R_2^St_2\right) \\ &\times \exp\left(-R_2^+|t_2+t_1-t_{1\max}|\right)(t_1=0\sim t_{1\max}, t_2=0\sim t_{1\max}), \end{aligned} \tag{4}$$

where R_2^I and R_2^S are the transverse relaxation rates of I and S, respectively. R_2^+ is the transverse relaxation rate due to inhomogeneous broadening. In an *in vivo* case, the formula $R_2^S \ll R_2^I \ll R_2^+$ is tenable [14]. The term $\exp\left(-R_2^+|t_2+t_1-t_{1\max}|\right)$ shows that the signal is an echo attenuated due to the field inhomogeneities, and has a maximum magnitude at $t_1 + t_2 = t_{1\max}$ when the phase divergence $\Delta\omega t$ is canceled. However, the CT-iDH-iZQC signal is not a complete echo due to the R_2^I and R_2^S. The mirror image of the CT-iDH-iZQC signal with respect to $t_1 = 0$ can be obtained by reversing the sign of t_1:

$$\begin{aligned} &\overset{t_1\to -t_1}{\to} \frac{i}{4}I_zS^- \exp(i\Omega_It_1) \exp\left(R_2^It_1\right) \exp(-i\Omega_St_2) \\ &\quad\times \exp\left(-R_2^St_2\right) \exp\left(-R_2^+|t_2-t_1-t_{1\max}|\right)(t_1 \\ &\quad= -t_{1\max}\sim 0, t_2=0\sim t_{1\max}). \end{aligned} \tag{5}$$

Similar to the deduction of the CT-iDH-iZQC signal, the CT-iDH-iDQC signal can be deduced as:

$$
\begin{aligned}
I_zS_z &\xrightarrow{\frac{\pi}{2}I_x,\frac{\pi}{2}S_x} \frac{1}{4}I^+S^+ \xrightarrow{t_1} \frac{1}{4}I^+S^+\exp[i(\Omega_S+\Omega_I)t_1]\\
&\times \exp\left[-\left(R_2^I+R_2^S\right)t_1\right] \xrightarrow{\pi I_x} \frac{1}{4}I^-S^+\exp[i(\Omega_S+\Omega_I)t_1]\\
&\times \exp\left[-\left(R_2^I+R_2^S\right)t_1\right] \xrightarrow{\frac{\pi}{2}I_x} \frac{i}{4}I_zS^+\exp[i(\Omega_S+\Omega_I)t_1]\\
&\times \exp\left[-\left(R_2^I+R_2^S\right)t_1\right] \xrightarrow{-t_1} \frac{i}{4}I_zS^+\exp(i\Omega_It_1)\\
&\times \exp\left(-R_2^It_1\right) \xrightarrow{\pi I_x,\pi S_x,t_2} \frac{i}{4}I_zS^-\exp(i\Omega_It_1)\\
&\times \exp\left(-R_2^It_1\right)\exp(-i\Omega_St_2)\exp\left(-R_2^St_2\right)\\
&\times \exp\left(-R_2^+|t_2-t_1-t_{1\max}|\right)(t_1=0\sim t_{1\max},t_2=t_{1\max}\sim 2t_{1\max}),
\end{aligned}
\tag{6}
$$

where the term $\exp\left(-R_2^+|t_2-t_1-t_{1\max}|\right)$ shows that the echo signal has a maximum magnitude when $t_1 - t_2 = t_{1\max}$. Superposition of the mirror image signal of CT-iDH-iZQC and the signal of CT-iDH-iDQC gives

$$
\begin{aligned}
&\xrightarrow{(5)+(6)} \frac{i}{4}I_zS^-\exp(i\Omega_It_1)\exp\left(R_2^I|t_1|\right)\exp(-i\Omega_St_2)\\
&\times \exp\left(-R_2^St_2\right)\exp\left(-R_2^+|t_2-t_1-t_{1\max}|\right)\\
&\times (t_1=-t_{1\max}\sim t_{1\max},t_2=0\sim 2t_{1\max}).
\end{aligned}
\tag{7}
$$

where the signal is almost an echo centered at $(t_1,t_2) = (0,t_{1\max})$ when R_2^S is ignored. For convenience for FT in later procedure, a left shift along t_2 by $t_{1\max}$ is performed to translate the signal to center at the origin of a new coordinate system (t_1, t_2'):

$$
\begin{aligned}
&\xrightarrow{t_2'=t_2-t_{1\max}} \frac{i}{4}I_zS^-\exp(i\Omega_It_1)\exp\left(-R_2^I|t_1|\right)\exp\left[-i\Omega_S(t_2'+t_{1\max})\right]\\
&\times \exp\left[-R_2^S(t_2'+t_{1\max})\right]\exp\left(-R_2^+|t_2'-t_1|\right)(t_1,t_2'=-t_{1\max}\sim t_{1\max}),
\end{aligned}
\tag{8}
$$

which shows that the effects of field inhomogeneity $\Delta\omega$ exist in both t_1 and t_2 dimensions. To get a high-resolution projected signal on the ω_2 axis, a shearing along t_1 by $\pi/4$ is required:

$$
\begin{aligned}
&\xrightarrow{t_1'=t_1-t_2'} \frac{i}{4}I_zS^-\exp\left[i\Omega_I(t_1'+t_2')\right]\exp\left(-R_2^I|t_1'+t_2'|\right)\\
&\times \exp\left[-i\Omega_S(t_2'+t_{1\max})\right]\exp\left[-R_2^S(t_2'+t_{1\max})\right]\\
&\times \exp\left(-R_2^+|t_1'|\right)(t_2'=-t_{1\max}\sim t_{1\max})\\
&= \frac{i}{4}I_zS^-\exp(i\Omega_It_1')\exp\left[-R_2^I|t_1'+t_2'|\right]\exp\left(-R_2^+|t_1'|\right)\\
&\times \exp\left[-i(\omega_S-\omega_I)t_2'\right]\exp(-i\Omega_St_{1\max})\\
&\times \exp\left[-R_2^S(t_2'+t_{1\max})\right](t_2'=-t_{1\max}\sim t_{1\max}),
\end{aligned}
\tag{9}
$$

which shows that the signal is free of inhomogeneous broadening in the t_2' dimension after the shearing. Since $R_2^I \ll R_2^+$, t_1' is ignored in $\exp(-R_2^I|t_1'+t_2'|)$ when compared to $\exp(-R_2^+|t_1'|)$. Next, complex FT with respect to t_1' is performed:

$$
\begin{aligned}
&\xrightarrow{R_2^I\ll R_2^+,FT(t_1')} iI_zS^-\frac{R_2^+}{(\omega_1-\Omega_I)^2+R_2^{+2}}\exp[-i(\omega_S-\omega_I)t_2']\exp(-i\Omega_St_{1\max})\\
&\times \exp(-R_2^I|t_2'|)\exp\left[-R_2^S(t_2'+t_{1\max})\right](t_2'=-t_{1\max}\sim t_{1\max}).
\end{aligned}
\tag{10}
$$

Since the relaxation rate of tissue water is usually one magnitude larger than most metabolites in organism in *in vivo* case, i.e. $R_2^S \ll R_2^I$, $\exp(-R_2^St_2')$ is ignored. Finally, complex FT with respect to t_2' is performed:

$$
\begin{aligned}
&\xrightarrow{R_2^S\ll R_2^I,FT(t_2')} iI_zS^-\frac{R_2^+}{(\omega_1-\Omega_I)^2+R_2^{+2}}\exp(-i\Omega_St_{1\max})\\
&\times \exp\left(-R_2^St_{1\max}\right)\frac{R_2^I}{(\omega_2+\omega_S-\omega_I)^2+R_2^{I2}} \xrightarrow{absolute\,value} I_zS^-\\
&\times \exp\left(-R_2^St_{1\max}\right)\frac{2R_2^+}{(\omega_1-\Omega_I)^2+R_2^{+2}}\\
&\times \frac{2R_2^I}{(\omega_2+\omega_S-\omega_I)^2+R_2^{I2}}.
\end{aligned}
\tag{11}
$$

An absorption-mode spectrum is therefore obtained with absolute value mode. The illustration to obtain double-absorption iMQC spectrum using the experimental time-domain signal of the aspartate sample is shown in Fig. 2.

Phasing is a minor problem that should be considered in obtaining absorption spectra, that is, multiplying P-type and N-type signals by $\exp(i\varphi_P)$ and $\exp(i\varphi_N)$, respectively, where φ_P and φ_N are the phase deviations or errors or shifts from P and N CTPs, respectively:

$$
\begin{aligned}
\varphi_P &= (-\Omega_I+\Omega_S)\tau_1+(\Omega_I+\Omega_S)\tau_2+\Omega_S\tau_3-\Omega_S\tau_4+\phi\\
\varphi_N &= (\Omega_I+\Omega_S)\tau_1+(-\Omega_I+\Omega_S)\tau_2+\Omega_S\tau_3-\Omega_S\tau_4+\phi
\end{aligned}
\tag{12}
$$

where ϕ is the zero-order phase deviation. Different phase deviations associated with initial delays (zero-order) and CTPs (first-order) will result in phase distortions that cannot be removed by conventional phase correction procedures. This problem can be easily solved with $\tau_1 = \tau_2$.

2.2. Elimination of strong coupling artifacts

For strong coupled systems, the hard π pulse leads to coherence transfer between t_1 and t_2, and produces cross-peaks [24]. It seems that additional cross-peaks may appear as strong coupling

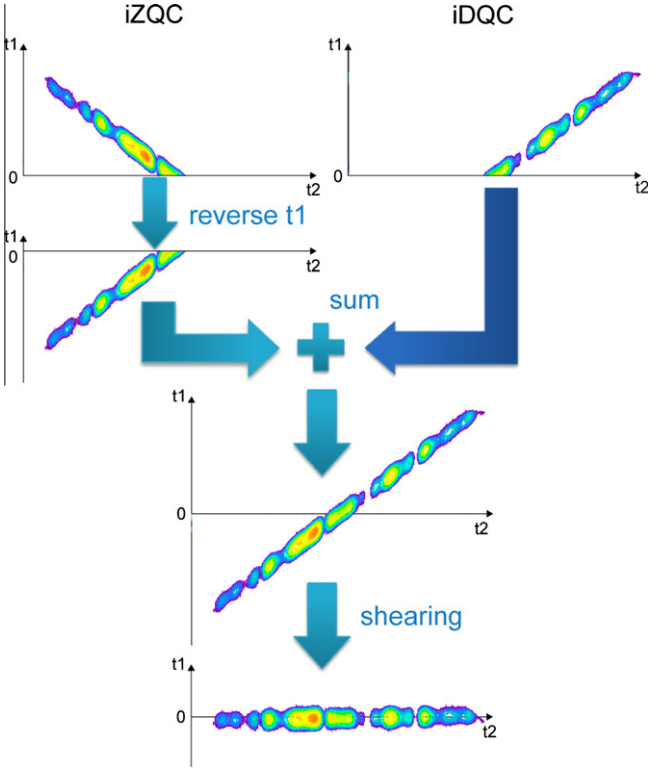

Fig. 2. Illustration to obtain double-absorption iMQC spectrum using the experimental time-domain signal of the aspartate sample.

artifacts. This is true for conventional iMQC spectra. However, the CT-iDH sequence is designed with a constant t_1 evolution time when the solute precessions under frequency offsets and J-couplings remain invariant, because no other RF pulse is exerted on the solute spins. Therefore, the frequency offsets and J-couplings of solute will not cause t_1-modulation. Despite that cross-peaks do exist due to the hard π pulse, they have the same t_2-precessions as axial peaks and will exactly overlap each other. Consequently, no extra strong coupling artifacts will appear in the CT-iDH spectra. Therefore, the multiplet patterns and relative intensities of each multiplet in a CT-iDH spectrum and its projection are the same as those in conventional 1D single-quantum coherence (SQC) spectra. While in conventional iMQC spectra under inhomogeneous fields, additional strong coupling artifacts appear. Therefore, in their projected spectra to achieve high-resolution, two problems maybe arise. Firstly, the relative intensities of each multiplet are different from natural values because projections are calculated from absolute-value spectra regardless of their alternating signs. Secondly, in non-iZQC spectra which have inhomogeneous line broadening in both dimensions, shearing is required to remove the inhomogeneous broadening in one dimension. In such cases, the peak number of a muliplet will increase in the projection after shearing. This problem does not appear in iZQC spectra which are free from field inhomogeneities in ω_1 axis and require no shearing to get high-resolution projections.

3. Experimental

All experiments were performed on an 11.74 T Varian NMR System with 54 mm narrow bore, using a 5 mm indirect detection probe at 298 K. Three samples were measured. Sample I was an aqueous solution phantom containing 1.2 mM aspartate (Asp); Sample II was an aqueous solution phantom containing 14 mM creatine (Cr), 4.5 mM lactate (Lac) and 4.5 mM citrate (Cit); Sample III was an intact pig brain tissue fitted in a 5 mm NMR tube. They were used to demonstrate implementation details of the new method. For Samples I and II, the Z1 shimming coil was deliberately deshimmed to produce a linewidth of 40 Hz to simulate the static field inhomogeneity. The excitation sculpting scheme [25,26] of two frequency selective refocusing pulses and two pairs of spoiling gradients was used as the water suppression (WS) module. The W5 composite pulse [27] was used for the water-exclusive π pulse right before the iDQF period and the two water-exclusive π pulses in the WS module. The parameters (strength $\times$ duration) of CSGs were G' = 0.07 T/m $\times$ 1.2 ms, G = 0.16 T/m $\times$ 1.2 ms, G_1 = 0.14 T/m $\times$ 1.0 ms, and G_2 = 0.24 T/m $\times$ 1.0 ms, respectively, where G_1 and G_2 are the spoiling PFGs in the WS module. An 8-step phase cycling was applied for the CT-iDH sequences: $\theta = (x, y, -x, -y, x, y, -x, -y)$, $\varphi = (x, x, x, x, -x, -x, -x, -x)$ and receiver = $(x, -x, x, -x, x, -x, x, -x)$, where φ is the phase of the water-exclusive π pulses in the WS module. The phase cycling for the first RF pulse of the original iZQC/iDQC sequences is: $\theta = (x, y, -x, -y, x, y, -x, -y)$. The repetition time (TR, defined as the duration of between two averages) and the spin echo time (TE, defined as the duration from the excitation to the echo maximum) were TR/TE = 2000/420 ms. $\tau_1 = \tau_2 = \tau_4 = 0$; $\tau_3 = t_{1max}$ = 200 ms. 500 $\times$ 25 points were acquired with spectral widths of 5000 Hz $\times$ 120 Hz in $F_2 \times F_1$ dimensions in ca. 16 min. For brain tissue sample, TR/TE = 2000/220 ms. $\tau_3 = t_{1max}$ = 100 ms. 500 $\times$ 10 points were acquired with spectral widths of 5000 Hz $\times$ 100 Hz in the F2 $\times$ F1 dimensions in ca. 20 min.

4. Results and discussion

For the sample of aspartate (Asp) in aqueous solution, the ratio of proton numbers of Asp and water is about 1:10,000. It is known that the protons in Asp form a typical ABX spin system. The different iMQC high-resolution spectra of AB part are presented in Fig. 3. Fig. 3a shows the high-resolution 1D spectrum under a well shimmed field (green) and conventional 1D spectrum under an inhomogeneous field with a linewidth of 40 Hz (red), in which the multiplet of eight lines cannot be resolved at all. Fig. 3b is the original iZQC spectrum with the projection onto the F1 dimension acquired with the pulse sequence shown in Fig. 1a under the same inhomogeneous field. It can be seen that a high-resolution projection spectrum free of inhomogeneous broadening can be obtained in the F1 dimension. However, eight strong coupling artifacts marked in blue exist in the 2D spectrum. The eight desired "diagonal-peaks" are marked in red. The undesired resonances are due to the coherence transfer between strongly coupled spins caused by the π pulse in the original iZQC sequence (Fig. 1a). Because the strong coupling cross-peaks are displayed in absolute-value mode, they lead to distortions of the projection intensities of resonances. The influence of the strong coupling artifacts is more severe in the original iDQC high-resolution spectrum. The iDQC spectrum (Fig. 3c) was acquired under the same experimental condition as Fig. 3a and b. After the shearing process and projection (Fig. 3d), it can be seen that the strong coupling cross-peaks (marked in blue[1]) no longer present in the same frequencies of the corresponding diagonal resonances. As a result, the strong coupling cross-peaks in the 2D spectrum result in additional resonances in the F1 projection spectrum. There are 16 resonances in the projection spectrum instead of 8. Therefore, the strong coupling effect in either iZQC or iDQC spectrum may lead to misinterpretation or incorrect quantification of sample. The CT-iDH-iZQC spectrum is presented in Fig. 3e. Because of the utilization of the CT scheme, the cross- and diagonal-peaks overlap in the 2D spectrum, thus there is no observable strong coupling artifact. The projection spectrum holds an intensity pattern similar to the conventional 1D SQC spectrum and the interpretation and quantification can be well performed. The dispersion parts of resonances in the CT-iDH-iDQC and CT-iDH-iZQC spectra can cancel each other, so a pure-phase 2D spectrum can be obtained. The result is presented in Fig. 3f. Similar to the CT-iDH-iDQC and CT-iDH-iZQC spectra, there is no observable strong coupling artifact in the 2D CT-iDH-absorption spectrum. Furthermore, since the dispersion parts are eliminated, the resolution of the CT-absorption spectrum is improved by two times. An ultrahigh-resolution spectrum can be obtained from the F1 projection.

Fig. 4 shows the comparison of original iZQC, CT-iDH-iZQC, and CT-absorption spectra under an inhomogeneous field and conventional 1D spin-echo spectrum in a homogeneous field. The sample is 14 mM creatine (Cr), 4.5 mM lactate (Lac) and 4.5 mM citrate (Cit) in aqueous solution. Different spin systems: singlet (Cr), weakly-coupled multiplets (Lac), strongly-coupled multiplets (Cit) are included in the sample so that we can compare the efficiency of different sequences. A same spin echo time, TE = 420 ms, was applied for all the sequences. The comparisons of the peak linewidth, the signal sensitivity and the peak height ratio of Cit from different sequences are listed in Table 1.

The conventional spin-echo spectrum under a well-shimmed static magnetic field (Fig. 4e) was acquired as a control spectrum. Compared to the spin-echo spectrum in Fig. 4e, the strongly-coupled multiplets of citrate (AB spin system) in the original iZQC spectrum (Fig. 4b) are distorted in the resonance intensities: the two outside resonances are 68% and 61% higher than the ones in the conventional spin-echo spectrum (Table 1). Furthermore, with the same acquisition time, the peak linewidth of the iZQC spectrum

[1] For interpretation of color in Figs. 2–4, the reader is referred to the web version of this article.

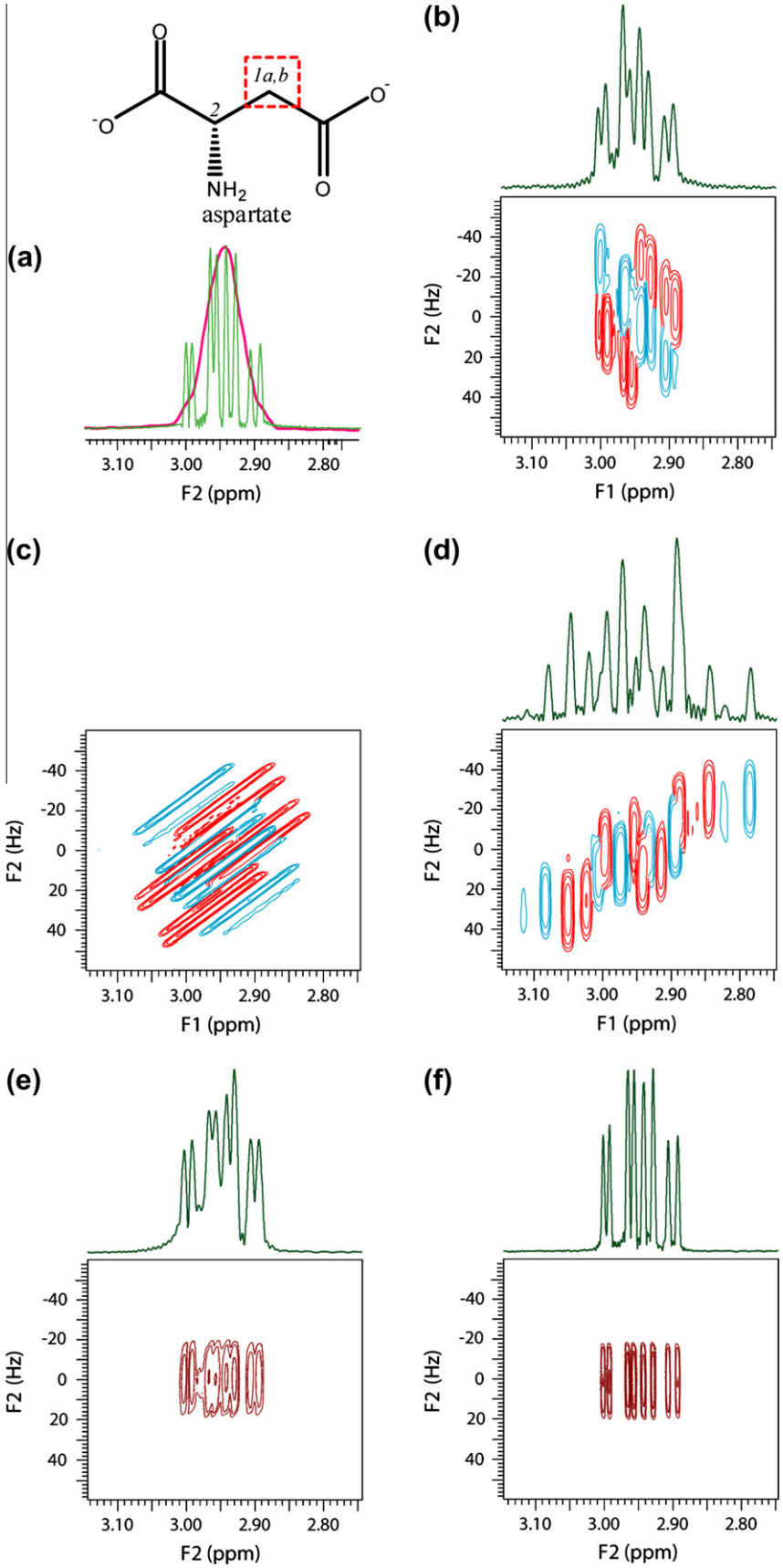

Fig. 3. ^{1}H spectra of AB part of Asp in aqueous solution in an inhomogeneous field with a linewidth of 40 Hz. (a) Conventional spin-echo spectrum (red); (b) original iZQC spectrum; (c and d) original iDQC spectra before (c) and after (d) shearing, where the diagonal peaks are marked in red, while the undesired cross-peaks caused by strong coupling are marked in blue; (e) CT-iDH-iZQC spectrum; and (f) CT-iDH-absorption spectrum, which combines CT-iDH-iZQC and -iDQC. Conventional spin-echo spectrum in a well-shimmed magnetic field is also presented in (a) for reference (green).

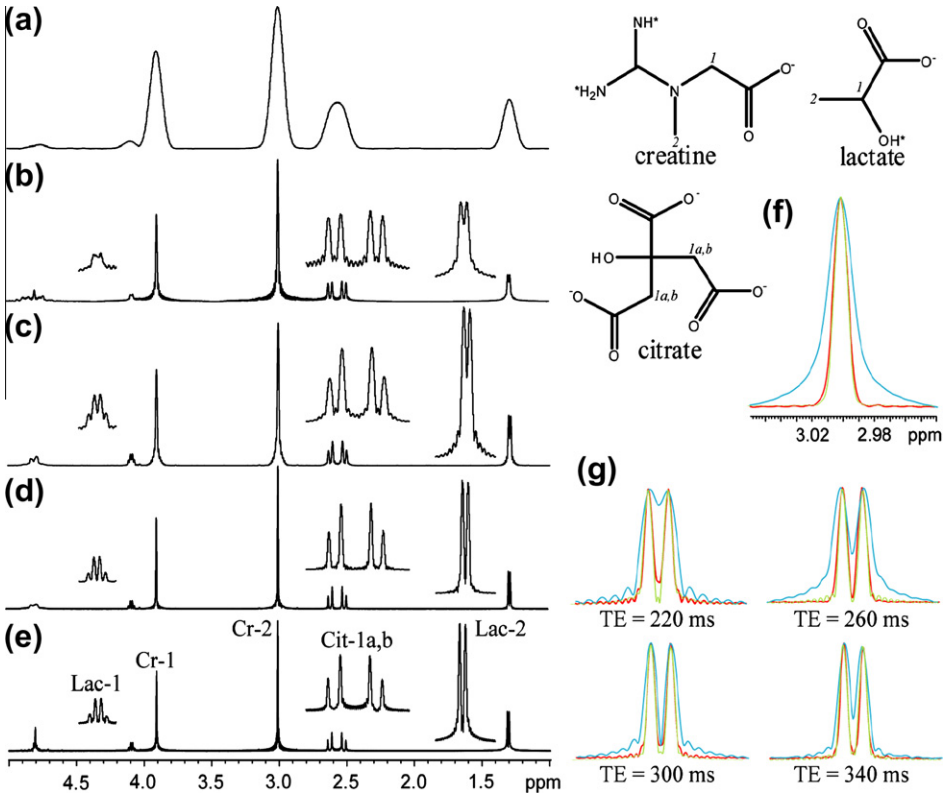

Fig. 4. [1]H spectra of Cr, Lac and Cit in aqueous solution. (a) Conventional spin-echo spectrum, (b) original iZQC projection spectrum; (c) CT-iDH-iZQC projection spectrum; (d) CT-iDH-absorption projection spectrum. (a–d) are all acquired under an inhomogeneous field with a linewidth of 40 Hz. (e) 1D conventional spin-echo spectrum in a homogeneous field; (f and g) Cr singlet (f) and Lac doublet (g) under different spin-echo times of CT-iDH-iZQC projection spectra (blue), CT-iDH-absorption projection spectra (red) and high-resolution spin-echo spectra (green).

Table 1
Peak linewidth, signal sensitivity and peak height ratio of Cit from different sequences.

	iZQC[d]	CT-iDH[d]			Spin-echo[e]
		iZQC	iDQC	Absorption	
FWHM[a] (Hz)	6.4	7.2	6.5	3.8	3.2
Sensitivity[b]	0.14	0.11	0.14	0.15	1.00
Peak height ratio of Cit[c]	0.89	0.60	0.59	0.58	0.53
	0.96	0.98	0.99	0.99	0.96
	1.00	1.00	1.00	1.00	1.00
	0.92	0.60	0.60	0.59	0.57

[a] The full width at half maximum (FWHM) of Cr (3.0 ppm) is measured.
[b] The sensitivity is defined as SNR/$\sqrt{\text{acquisition time}}$, normalized to the one of spin-echo spectrum.
[c] Normalized to the highest resonance of Cit in each spectrum.
[d] Under inhomogeneous fields with a linewidth of 40 Hz.
[e] Under a well shimmed magnetic field.

is increased by two times compared to the spin-echo spectrum (Table 1). Fig. 4c is the CT-iDH-iZQC spectrum. Though the spectral resolution of the CT-iDH-iZQC spectrum remains the same as the iZQC spectrum, the strongly-coupled multiplets have similar intensity pattern to the one in Fig. 4e (the deviations of outer two lines are 13% and 5%, respectively). In the CT-iDH-absorption spectrum (Fig. 4d), not only the correct multiplet intensity pattern is preserved (the deviations of outer two lines are 9% and 4%, respectively), but also the spectral linewidth is reduced by almost half, which is similar to that of the spin-echo spectrum. Fig. 4f and g give lineshape comparisons of the Cr singlet at 3.0 ppm and the weakly coupled Lac doublet, respectively, of CT-iDH-iZQC, CT-iDH-absorption, and well-shimmed spin-echo spectra under different spin echo times. It can be seen that the absorption spectroscopy greatly alleviates the lineshape variations of multiplets due to *J*-modulation. The improved spectral resolution and the correct multiplet intensity pattern ensure a more accurate quantification of compound concentrations.

Fig. 5 presents the preliminary results on an *in vitro* pig brain tissue. The spectra shown in Fig. 5a–c are from conventional spin-echo sequence, original iZQC sequence, and CT-iDH sequence respectively with a same spin echo time of 120 ms. It can be seen that the spectral inhomogeneous broadening is greatly suppressed in the original iZQC spectrum. However, its ultimate spectral resolution is restricted by the very short relaxation time of tissue water [14]. The CT-iDH sequence alleviates this problem and further improves the resolution doubly. To our knowledge, it is the first time that iMQC spectroscopy achieves a linewidth less than

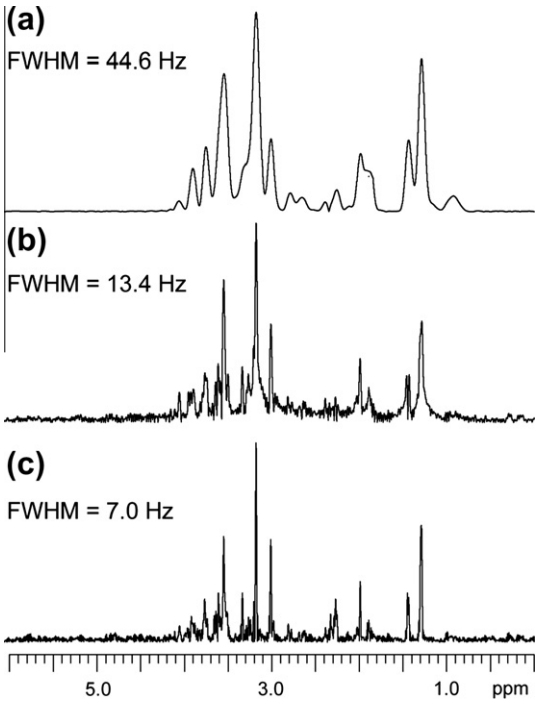

Fig. 5. Spin echo spectrum (a), original iZQC projection spectrum (b), and CT-iDH projection spectrum (c) of a same pig brain tissue with a spin echo time of 120 ms.

10 Hz on intact animal tissues. The iMQC spectra shown in Fig. 5b and c look much noisy than conventional one. This may be mainly caused by inherent low signal intensity of iMQCs and short transverse relaxation time of tissue water.

5. Conclusions

In summary, a pulse sequence utilizing both CT-iZQC and CT-iDQC coherence transfer pathways to obtain 2D absorption-mode lineshape was proposed and theoretically analyzed. Experimental results on solution phantoms and intact animal tissue demonstrate that higher resolution and more straightforward spectral information can be revived. The new scheme not only improves the spectral resolution by two times, but also effectively suppresses the strong coupling artifacts and distortion of multiplet intensity pattern. This approach is applicable to weakly-coupled, strongly-coupled and uncoupled spin systems, potentially useful for studying metabolites in *in vivo* NMR spectroscopy and for characterizing technologically important new materials in combinatorial chemistry.

Acknowledgments

This work was partially supported by the NNSF of China under Grants 10974164, 11074209 and 11105114, the Fundamental Research Funds for the Central Universities under Grant 2010121010 and the Research Fund for the Doctoral Program of Higher Education of China under Grant 200803840019.

References

[1] C.A. Meriles, D. Sakellariou, H. Heise, A.J. Moulé, A. Pines, Approach to high-resolution *ex situ* NMR spectroscopy, Science 293 (2001) 82–85.
[2] J. Perlo, V. Demas, F. Casanova, C.A. Meriles, J. Reimer, A. Pines, B. Blümich, High-resolution NMR spectroscopy with a portable single-sided sensor, Science 308 (2005) 1279.
[3] J. Perlo, F. Casanova, B. Blümich, *Ex situ* NMR in highly homogeneous fields: ^{1}H spectroscopy, Science 315 (2007) 1110–1112.
[4] D. Topgaard, R.W. Martin, D. Sakellariou, C.A. Meriles, A. Pines, "Shim pulses" for NMR spectroscopy and imaging, Proc. Natl. Acad. Sci. USA 101 (2004) 17576–17581.
[5] B. Blümich, J. Perlo, F. Casanova, Mobile single-sided NMR, Prog. Nucl. Magn. Reson. Spectrosc. 52 (2008) 197–269.
[6] P. Pelupessy, E. Rennella, G. Bodenhausen, High-resolution NMR in magnetic fields with unknown spatiotemporal variations, Science 324 (2009) 1693–1697.
[7] E. Danieli, J. Perlo, B. Blümich, F. Casanova, Small magnets for portable NMR spectrometers, Angew. Chem. Int. Ed. 49 (2010) 4133–4135.
[8] W.S. Warren, W. Richter, A.H. Andreotti, B.T. Farmer, Generation of impossible cross-peaks between bulk water and biomolecules in solution NMR, Science 262 (1993) 2005–2009.
[9] S. Vathyam, S. Lee, W.S. Warren, Homogeneous NMR spectra in inhomogeneous fields, Science 272 (1996) 92–96.
[10] Z. Chen, Z.W. Chen, J.H. Zhong, High-resolution NMR spectra in inhomogeneous fields via IDEAL (intermolecular dipolar-interaction enhanced all lines) method, J. Am. Chem. Soc. 126 (2004) 446–447.
[11] D.Z. Balla, G. Melkus, C. Faber, Spatially localized intermolecular zero-quantum coherence spectroscopy for *in vivo* applications, Magn. Reson. Med. 56 (2006) 745–753.
[12] D.Z. Balla, C. Faber, *In vivo* intermolecular zero-quantum coherence MR spectroscopy in the rat spinal cord at 17.6 T: a feasibility study, Magn. Reson. Mater. Phys. Biol. Med. 20 (2007) 183–191.
[13] D.Z. Balla, C. Faber, Intermolecular zero-quantum coherence NMR spectroscopy in the presence of local dipole fields, J. Chem. Phys. 128 (2008) 154522.
[14] X. Chen, M.J. Lin, Z. Chen, S.H. Cai, J.H. Zhong, High-resolution intermolecular zero-quantum coherence spectroscopy under inhomogeneous fields with effective solvent suppression, Phys. Chem. Chem. Phys. 9 (2007) 6231–6240.
[15] X. Chen, M.J. Lin, Z. Chen, J.H. Zhong, Fast acquisition scheme for achieving high-resolution MRS with *J*-scaling under inhomogeneous fields, Magn. Reson. Med. 61 (2009) 775–784.
[16] M.J. Lin, X. Chen, S.H. Cai, Z. Chen, High-resolution magnetic resonance spectroscopy in unstable fields via intermolecular zero-quantum coherences, Phys. Chem. Chem. Phys. 12 (2010) 6014–6020.
[17] M.J. Lin, Y.Q. Huang, X. Chen, S.H. Cai, Z. Chen, High-resolution 2D NMR spectra in inhomogeneous fields based on intermolecular multiple-quantum coherences with efficient acquisition schemes, J. Magn. Reson. 208 (2011) 87–94.
[18] A.J. Pell, R.A.E. Edden, J. Keeler, Broadband proton–decoupled proton spectra, Magn. Reson. Chem. 45 (2007) 296–316.
[19] A.J. Pell, J. Keeler, Two-dimensional *J*-spectra with absorption-mode lineshapes, J. Magn. Reson. 189 (2007) 293–299.
[20] G. Wider, R. Baumann, K. Nagayama, R.R. Ernst, K. Wuthrich, Strong spin–spin coupling in the two-dimensional *J*-resolved 360-MHz ^{1}H NMR spectra of the common amino acids, J. Magn. Reson. 42 (1981) 73–87.
[21] M.J. Thrippleton, R.A.E. Edden, J. Keeler, Suppression of strong coupling artefacts in *J*-spectra, J. Magn. Reson. 174 (2005) 97–109.
[22] N. Nagayama, A. Kumar, K. Wuthrich, K.K. Ernst, Experimental techniques of two-dimensional correlated spectroscopy, J. Magn. Reson. 40 (1980) 321–334.
[23] P. Bachmann, W.P. Aue, L. Muller, R.R. Ernst, Phase separation in two-dimensional spectroscopy, J. Magn. Reson. 28 (1977) 29–39.
[24] G. Bodenhausen, R. Freeman, G.A. Morris, D.L. Turner, NMR spectra of some simple spin systems studied by two-dimensional Fourier transformation of spin echoes, J. Magn. Reson. 31 (1978) 75–95.
[25] T.L. Hwang, A.J. Shaka, Water suppression that works – excitation sculpting using arbitrary wave-forms and pulsed-field gradients, J. Magn. Reson. 112 (1995) 275–279.
[26] G. Zheng, W.S. Price, Solvent signal suppression in NMR, Prog. Nucl. Magn. Reson. Spectrosc. 56 (2010) 267–288.
[27] M.L. Liu, X.A. Mao, C.H. Ye, H. Huang, J.K. Nicholson, J.C. Lindon, Improved WATERGATE pulse sequences for solvent suppression in NMR spectroscopy, J. Magn. Reson. 132 (1998) 125–129.